

# SIR-Hawkes: on the Relationship Between Epidemic Models and Hawkes Point Processes

Marian-Andrei Rizoiiu  
ANU & Data61 CSIRO  
Canberra, Australia

Swapnil Mishra  
ANU & Data61 CSIRO  
Canberra, Australia

Quyu Kong  
ANU  
Canberra, Australia

Mark Carman  
Monash University  
Melbourne, Australia

Lexing Xie  
ANU & Data61 CSIRO  
Canberra, Australia

## ABSTRACT

Two of the main frameworks used for modeling information diffusions in the online are epidemic models and Hawkes point processes. The former consider information as a viral contagion which spreads into a population of online users, and employ tools initially developed in the field of epidemiology. The latter view individual broadcasts of information as events in a point process and they modulate the event rate according to observed (or assumed) social principles; they have been broadly used in fields such as finance and geophysics. Here, we study for the first time the connection between these two mature frameworks, and we find them to be equivalent. More precisely, the rate of events in the Hawkes model is identical to the rate of new infections in the Susceptible-Infected-Recovered (SIR) model when taking the expectation over recovery events – which are unobserved in a Hawkes process. This paves the way to apply tools developed for one framework across the gap, to the other framework.

We make three further contributions in this work. First, we propose HawkesN, an extension of the basic Hawkes model, in which we introduce the notion of finite maximum number of events that can occur. Second, we show HawkesN to explain real retweet cascades better than the current state-of-the-art Hawkes modeling. The size of the population can be learned while observing the cascade, at the expense of requiring larger amounts of training data. Third, we employ an SIR method based on Markov chains for computing the final size distribution for a partially observed cascade fitted with HawkesN. We propose an explanation to the generally perceived randomness of online popularity: the final size distribution for real diffusion cascades tends to have two maxima, one corresponding to large cascade sizes and another one around zero.

### ACM Reference format:

Marian-Andrei Rizoiiu, Swapnil Mishra, Quyu Kong, Mark Carman, and Lexing Xie. 1997. SIR-Hawkes: on the Relationship Between Epidemic Models and Hawkes Point Processes. In *Proceedings of arXiv submission, Canberra, Australia, 2017, Nov. 2017 (arXiv'18)*, 16 pages.  
[https://doi.org/10.475/123\\_4](https://doi.org/10.475/123_4)

## 1 INTRODUCTION

The research community has long been aware of the importance of the word-of-mouth phenomenon in information dissemination

and in shaping consumer behavior [14]. This is especially true nowadays, with the advent of the online environment and social media. In this paper, we study how information spreads online by modeling its underlying mechanism, i.e. how it passes from individual to individual. The aim is to link individual actions to collective-level measures, such as popularity or fame.

This work addresses three open questions concerning the classes of approaches mainly used for modeling online diffusions: *epidemic models* and *Hawkes point processes*. The first question is about designing more expressive diffusion models. Hawkes processes are the de facto modeling choice for social media processes, mainly because they can be easily customized to account for social factors such as the influence of users [15, 44], the length of “social memory” [23, 30] and the inherent content quality [22]. **Is it possible to use insights from both classes of approaches to design enhanced diffusion models?** In particular, can we employ notions from epidemic models to design a Hawkes process more adept at describing online diffusions? The second open question regards the relationship between the two classes of models. Epidemic models emerged from the field of epidemiology, and consider information as a viral contagion which spreads within a population of online users; Hawkes models have been mainly used in finance and geophysics, and view individual broadcasts of information as events in a stochastic point process. **Given the two classes of approaches emerged from very different research fields, can we draw a connection between them?** The third question concerns the range of tools that can be employed with the two classes of models. Epidemic models and Hawkes processes emerged from different fields, and very different outcomes were prioritized for each: epidemiology was mainly interested in the likelihood and the size of viral outbreaks [2, 5, 39], Hawkes processes were used for modeling and prediction [29] and designing interventions [28, 43]. **But can we apply the tools and techniques developed for one class of models, across the gap to the other class?**

In this work, we address all three questions above, by drawing for the first time the connection between epidemic models and point processes, validating it both theoretically and also empirically on three large publicly available datasets of retweet cascades.

To answer the first question, we propose HawkesN, an extension of the Hawkes model with a finite population. The basic Hawkes process [16] has no upper limit for the the number of events that may occur. This is hardly a realistic assumption for social media processes such as information diffusion, which relies on a finite underlying population of humans, each broadcasting a message a

finite number of times. We introduce the parameter  $N$ , denoting the maximum number of events that can occur in the point process, and we modulate the event rate by the available population. We show that the HawkesN model generalizes better to unseen data than the basic Hawkes model for real live diffusion cascades.

We answer the second question by studying the previously unexplored link between the Susceptible-Infected-Recovered (SIR) epidemic model [19] and the HawkesN model. The key to the link is the way they model the word-of-mouth process: each new broadcast from one user to another constitutes an event in HawkesN, and a new infection in SIR. The key to linking HawkesN and SIR models is the equivalence between an event in HawkesN and a new infection in SIR. Starting from this observation, we show that the rate of events in the HawkesN model is identical to the rate of new infections in the SIR model, when taking the expectation over recovery events – which are unobserved in the HawkesN process. Furthermore, we show that two of their most important quantities (the basic reproduction number for SIR and the branching factor for HawkesN) are also equivalent. This is significant, as it indicates that tools developed for one approach can be applied to the other.

To address the third question, we study the problem of predicting final cascade sizes. Previous work [23, 29, 30, 44] predict a single value for the expected future popularity, however it has been theorized that popularity has a random component [22] which affects the variance in prediction quality. We reconcile these two views by producing a probability distribution over future cascade size, by applying a Markov chain technique developed for SIR to a diffusion cascade which has been partially observed and fitted using HawkesN. Based on our observations on a large sample of real diffusion cascades, we also provide a nuanced explanation for the main-stream belief that popularity is unpredictable. For branching factor values around 2, shown by a large number of cascades in our real-life datasets, the distribution shows two peaks: the larger peak corresponds to the cascade extinguishing quickly after its beginning; the smaller peak corresponds to a large cascade size. At the beginning of the cascade it is impossible to distinguish between the two cases, however the posterior probability distribution after observing a prefix of the cascade can be updated to account for the observed events.

**The main contributions of this work include:**

- We introduce HawkesN – a novel class of Hawkes processes which have a number of events – and we show it generalizes better to unseen data than the state-of-the-art modeling.
- We show a previously unexplored connection between two different classes of approaches – epidemic models and Hawkes point processes – by showing that the proposed HawkesN model is mathematically equivalent in expectation to the SIR epidemic model;
- We use a Markov chain tool from epidemic model theory to predict the distribution of the final size of a cascade. We provide a nuanced explanation for the main-stream belief that popularity is unpredictable.

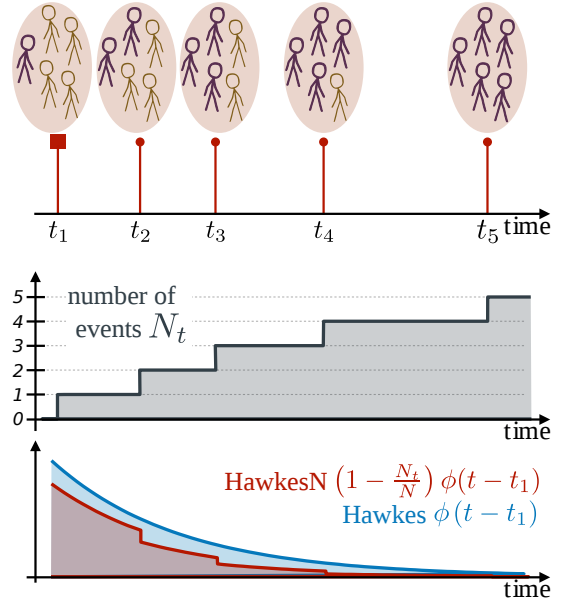


**Figure 1: An illustration of a diffusion in a population of five users. (top panel)** An event (say a tweet) is resulted from an action of a user (a user posts a tweet). Five events are depicted, having occurred at times  $t_j, j = 1..5$ . The state of the user population is shown at each time  $t_j$ : **purple users** have performed past observed events; **orange users** are yet to perform any action. **(middle panel)** The counting process  $N_t$  increases by one with each event; **(lower panel)** The rate of events generated by this first event (shown with a square tip), modeled by a basic Hawkes process [16] and by HawkesN.

## 2 HAWKESN: A PROCESS IN FINITE POPULATION

In this section, we propose a novel model, *HawkesN*, in which the underlying population that can participate in a point process is finite. To introduce notations and make the discussion self-contained, we begin with a brief review of point processes. In Sec. 2.3, we sketch the fitting procedures for HawkesN using maximum likelihood.

### 2.1 Poisson and Hawkes processes

A point process is a random process whose realizations consists of event times  $t_1, t_2, \dots$  falling along the non-negative line representing time [8], where  $t_j$  denotes the time of occurrence of the  $j$ -th event. The counting process  $N_t$  associated with the point process is a random function defined on time  $t \geq 0$  which counts the number of events of the point process up to time  $t$ . One can see that the set of event times  $t_j$  and the corresponding counting process  $N_t$  are equivalent representations of the underlying point process [8], with the event times being the time points where the (piece-wise constant) counting process increments in value.

**The Poisson process and its intensity.** A point process in which the inter-arrival times  $\tau_j = t_j - t_{j-1}$  are *i.i.d.* exponential random variables with parameter  $\lambda$  is called a homogeneous Poisson point process. For non-homogeneous Poisson processes,  $\lambda$  is

a function of time  $\lambda(t)$  and it is called the *event rate* of the Poisson process. It defines the probability of an event occurring in the infinitesimal interval around time  $t$ . Formally:

$$\begin{aligned}\mathbb{P}(N_{t+h} = n + m \mid N_t = n) &= \lambda(t)h + o(h) && \text{when } m = 1 \\ \mathbb{P}(N_{t+h} = n + m \mid N_t = n) &= o(h) && \text{when } m > 1 \\ \mathbb{P}(N_{t+h} = n + m \mid N_t = n) &= 1 - \lambda(t)h + o(h) && \text{when } m = 0\end{aligned}\quad (1)$$

where  $o(h)$  is a function so that  $\lim_{h \downarrow 0} \frac{o(h)}{h} = 0$ .

**The Hawkes process** [16] is a particular type of Poisson process, in which the occurrence of an event increases the likelihood of future events. The event rate for a Hawkes process is defined as:

$$\lambda(t) = \mu(t) + \sum_{t_j < t} \phi(t - t_j) \quad (2)$$

which models the following process: immigrant events arrive in the system at the rate of  $\mu(t)$ ; each previous event (immigrant or not) that occurred at time  $t_j$  generates new events at the rate  $\phi(t - t_j)$ .

**Branching factor.** One key quantity that described the Hawkes process is the branching factor  $n^*$ , defined as the expected number of child events directly spawned by an event. In the Hawkes process,  $n^*$  is indicative of the expected number of events. When  $n^* < 1$ , the process is in a *subcritical regime*: the number of events is bounded and the event rate  $\lambda(t)$  decays to zero over time. For  $n^* > 1$ , the process is in a *supercritical regime* and the number of events is infinite.

## 2.2 The HawkesN process

In this section, we propose a generalization of the Hawkes model [16] which allows limiting the maximum number of events that can occur in the process. To the best of our knowledge, no prior work on modeling social processes using Hawkes models had accounted for a finite underlying population.

**An extended Hawkes process.** We extend the basic Hawkes model by introducing a parameter  $N$  – the maximum number of events that can occur in the point process. The effect of the finite population size is that event rate is modulated by the available population. The event rate function in HawkesN is defined as:

$$\lambda^H(t) = \left(1 - \frac{N_t}{N}\right) \left[\mu(t) + \sum_{t_j < t} \phi(t - t_j)\right], \quad (3)$$

where  $\phi(t - t_j)$  can be the same kernel function used with the basic Hawkes, and  $N_t$  is the associated counting process.

The maximum number of events that could still occur after time  $t$  is  $N - N_t$ . The term  $1 - \frac{N_t}{N}$  scales the event rate at time  $t$  with the proportion of the events which can still occur after time  $t$ . When  $t = 0$ , we have  $\mathbb{E}[N_0] = \mu(0)$ ; when  $N_t \rightarrow N$ , we have  $\left(1 - \frac{N_t}{N}\right) \rightarrow 0$  and the event rate  $\lambda(t)$  converges to zero. This translates in a null probability of observing an event. Practically, the process dies out when  $N_t \rightarrow N$ .

Fig. 1 illustrates the HawkesN process for an information diffusion in a population of five users ( $N = 5$ ). Each user takes an action at most once, represented as event time  $t_j, j = 1..5$ . The corresponding counting process  $N_t$  is shown in the middle plot. Events  $t_2..t_5$  are considered to have been triggered by event  $t_1$ . The bottom panel compares the rate of events generated by  $t_1$  under a Hawkes model ( $= \phi(t - t_1)$ ) and the rate of events under the

HawkesN model ( $= \left(1 - \frac{N_t}{N}\right) \phi(t - t_1)$ ). In HawkesN, the population modulates the event rate by decreasing it after each new event. The event rate becomes zero after  $t_5$ , since the maximum number of events has been reached. Visibly, in the basic Hawkes we have  $\phi(t) > 0$ , for  $t \geq t_5$ , i.e. more events can potentially occur after  $t_5$ .

**Relation to the basic Hawkes.** When the maximum number of events is infinite ( $N \rightarrow \infty$ ), Eq. (3) simplifies to Eq. (2) defining the basic Hawkes process. In other words, the basic Hawkes process is a special case of the extended HawkesN model, in which  $N \rightarrow \infty$ .

**Kernel functions for online diffusions.** The exponential kernel  $\phi(\tau) = \theta e^{-\theta\tau}$  is a popular choice when modeling online social media [3, 9, 12, 23, 30, 43, 44]. Other kernel choices include power-law functions  $\phi(\tau) = (\tau + c)^{-(1+\theta)}$ , used in geophysics [17] and social networks [7, 20, 23] and the Reyleigh functions  $e^{-\frac{1}{2}\theta\tau^2}$ , used in epidemiology [35]. Here, we choose to use the modified exponential kernel function proposed by Mishra et al. [23], which captures the local influence of user in addition to the temporal decay:

$$\phi(\tau) = \kappa m^\eta \theta e^{-\theta\tau} \quad (4)$$

where  $m$  is the local user influence,  $\eta$  introduces a warping effect for the local user influence,  $\kappa$  is a scaler and  $\theta$  is the parameter of the exponential function. Note that for diffusion cascades the background intensity is zero  $\mu(t) = 0, \forall t > 0$  [23].

**Branching factor.** We define the branching factor of HawkesN as the expected number of children events directly spawned by the first event of the process. For large values of  $N$  and fast decaying kernel functions  $\phi(t)$ , we can approximate  $\frac{N_t}{N} \approx 0$  and therefore the branching factor for HawkesN is:

$$n^* \approx \int_1^\infty \int_0^\infty p(m) \kappa m^\eta \theta e^{-\theta\tau} d\tau dm = \kappa \frac{\alpha - 1}{\alpha - \eta - 1} \quad (5)$$

where  $p(m)$  is the distribution of local influence that Mishra et al. [23] studied on a large sample of tweets, and found to be a power-law of exponent  $\alpha = 2.016$ . In HawkesN, the branching factor is indicative of the speed at which the cascade unfolds and its final size distribution (as shown in Sec. 5.5).

## 2.3 Fitting HawkesN to observed data

The parameters of HawkesN can be estimated from observed data using a maximum likelihood procedure. The HawkesN process is completely defined by four parameters  $\{\kappa, \eta, \theta, N\}$ . The log-likelihood of observing a set of events  $\{(m_j, t_j), j = 1, \dots, n\}$  in a non-homogeneous Poisson process of event rate  $\lambda^H(t)$  is (see the online supplement [1] or Daley and Vere-Jones [8], Ch. 7.2):

$$\mathcal{L}(\kappa, \beta, c, \theta) = \sum_{j=1}^n \log \left( \lambda^H(t_j) \right) - \int_0^{t_n} \lambda^H(\tau) d\tau. \quad (6)$$

We detail further the integral term:

$$\begin{aligned}
\int_0^{t_n} \lambda^H(\tau) d\tau &= \int_0^{t_n} \left(1 - \frac{N_t}{N}\right) \sum_{t_j < t} \phi(t - t_j) dt \\
&= \sum_{j=1}^{n-1} \int_{t_j}^{t_n} \left(1 - \frac{N_t}{N}\right) \phi(t - t_j) dt \\
&= \sum_{j=1}^{n-1} \sum_{l=j}^{n-1} \frac{N - l}{N} \int_{t_l}^{t_{l+1}} \phi(t - t_j) dt \\
\text{cf. (4)} &= \kappa \sum_{j=1}^{n-1} (m_j)^\eta \sum_{l=j}^{n-1} \frac{N - l}{N} \left[ e^{-\theta(t_l - t_j)} - e^{-\theta(t_{l+1} - t_j)} \right]. \quad (7)
\end{aligned}$$

Eq. (6) is a non-linear objective that we maximize to find the set of parameters. There are a few natural constraints for each of the model parameters, namely:  $\theta > 0$ ,  $\kappa > 0$ , and  $0 < \eta < \alpha - 1$  for the branching factor to be defined. We use the mathematical modeling language AMPL [11], which offers a complete set of modeling tools, including automatic gradient computation and support for a large number of solvers. We choose as solver Ipopt [34], the state of the art optimizer for non-linear objectives. More details can be found in the online supplement [1].

### 3 LINKING HAWKESN AND SIR MODELS

We first establish a common language by reviewing a few key concepts in the SIR epidemic model. This allows us to link SIR models and Hawkes point processes – we show that the event rate of a HawkesN process is the same as the rate of new infections in the SIR model after averaging out unobserved recovery events.

#### 3.1 Background: the SIR Model

The Susceptible-Infected-Recovered (SIR) model defines three classes of individuals: those *susceptible* to infection, those currently *infected* (and therefore infectious) and those *recovered* from the infection and no longer infective. In a population of size  $N$ ,  $N = S(t) + I(t) + R(t)$ . Here  $S(t)$ ,  $I(t)$ , and  $R(t)$  are deterministic functions over time, and denote the respective size of each class at time  $t$ .

The SIR model assumes the following process: in a homogeneous population, individuals meet any other individual uniformly at random, at a rate  $\epsilon$ ; if during a meeting one of the individuals is infective and the other susceptible, then the latter will be infected with transmission probability  $\rho$ ; individuals recover from the infection at a constant rate  $\gamma$  – i.e. the times to recovery are exponentially distributed following  $\gamma e^{-\gamma t}$  and infections last on average  $\frac{1}{\gamma}$  units of time. We denote  $\beta = \epsilon\rho$ . SIR is governed by the following ordinary differential equations [2]:

$$\frac{dS(t)}{dt} = -\beta \frac{S(t)}{N} I(t) \quad (8)$$

$$\frac{dI(t)}{dt} = \beta \frac{S(t)}{N} I(t) - \gamma I(t) \quad (9)$$

$$\frac{dR(t)}{dt} = \gamma I(t) \quad (10)$$

**Model assumptions.** First, the basic SIR model assumes that the population is homogeneous and completely susceptible – meaning that all individuals are initially either in the susceptible pool or

infected ( $R(0) = 0$ ). Second, it assumes that all rates are constant: the contact rate  $\epsilon$ , the transmission rate  $\rho$ , and the recovery rate  $\gamma$ . Third, it assumes that the population has no births and no deaths. This assumption holds when the speed of the epidemic outpaces considerably the speed of change in the population – e.g., an average retweet diffusion only lasts minutes, compared to years of expected activity of a user on Twitter.

**The basic reproduction number** (denoted  $\mathcal{R}_0$ ) is the expected number of infections caused by a single infected individual at the start of the outbreak. Initially, almost all individuals in the population are susceptible  $S(0) \approx N$  and an infectious individual infects others at the constant rate of  $\beta \frac{S(t)}{N} \approx \beta$  for the duration of her infection (which lasts on average  $\frac{1}{\gamma}$ ). Intuitively,  $\mathcal{R}_0 = \beta/\gamma$ .  $\mathcal{R}_0 > 1$  is the necessary and sufficient condition to have a growing epidemic:

$$\frac{dI(0)}{dt} > 0 \stackrel{\text{Eq. (9)}}{\Leftrightarrow} \frac{\beta S(0)}{\gamma N} > 1 \stackrel{S(0) \approx N}{\Leftrightarrow} \mathcal{R}_0 = \frac{\beta}{\gamma} > 1. \quad (11)$$

**Stochastic SIR.** The model described so far is also known as the *deterministic SIR*. It describes the evolution of population sizes of the three classes. *Stochastic SIR* models behaviors of independent and identically distributed agents, whose actions are described by the same set of holistic rules defined in Eq. (8)-(10) [4]. The connection between the two variants is: the mean behavior of the stochastic process asymptotically approaching that of the deterministic process [2, 39]. Our own results on simulations of the two variants are presented in an online supplement [1]. As will be elaborated next, stochastic SIR provides the link to Hawkes point processes.

#### 3.2 SIR in expectation

First, we express stochastic SIR model as a bivariate Poisson process, and we derive the rate of new infections and the rate of new recoveries. Next, we compute the expected rate of new infections when the recovery events are unobserved. We show its connection with the event rate in a HawkesN process.

**Intuition.** When modeling information diffusion, both SIR and HawkesN model the same phenomenon: users come into contact with the diffused content, which they further broadcast to other users. Each new broadcast is modeled as a new event in HawkesN, and as a new infection in SIR. The key to linking HawkesN and SIR models is the equivalence between an event in HawkesN and a new infection in SIR. In HawkesN, past events generate new events at the rate  $\phi(t)$ , which is exponentially time-decaying in Eq. (4). In SIR, an infectious individual  $j$  infects susceptible individuals at a rate of  $\frac{\beta S(t)}{N}$  during its limited lifespan  $\tau_j$  – i.e. its *time to recovery*. As discussed in Sec. 3.1,  $\tau_j$  are exponentially distributed with the parameter  $\gamma$ . Intuitively, the expected rate of new infections in SIR (when taking expectation over the recovery times) is equal to the expected event rate in HawkesN with an exponential kernel.

Denote  $\tau = \{\tau_1, \tau_2, \dots\}$  as times to recovery of infected individuals in SIR;  $m = \{m_1, m_2, \dots\}$  as user influences in HawkesN;  $\alpha$  as the power-law exponent of user influence distribution (Eq. (5)). We now have Theorem 3.1.

**THEOREM 3.1.** *The new infections in a stochastic SIR process of parameters  $\{\beta, \gamma, N\}$  follow a non-homogeneous Poisson process of intensity  $\lambda^I(t)$ . Events in a HawkesN process with parameters  $\{\kappa, \eta, \theta, N\}$  follow has event intensity  $\lambda^H(t)$  (Eq 3). The expectation of  $\lambda^I(t)$*

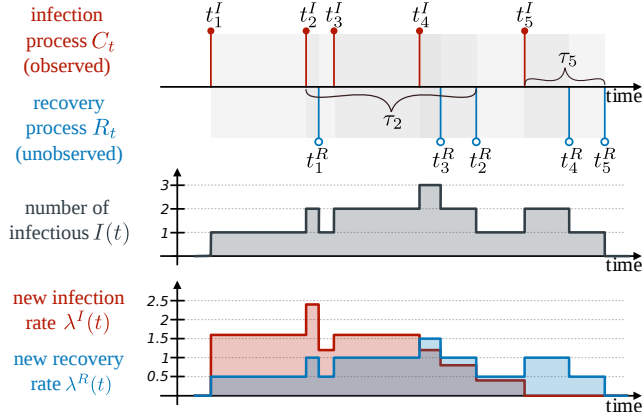


**Figure 2: An illustration of SIR as a bivariate Poisson process: the infection process and the recovery processes. (top panel)** Each of the five individuals gets infected at time  $t_j^I$  and recovers at  $t_j^R$ . Each individual  $j$  stays infectious for a period  $\tau_j$ . For the equivalence with HawkesN, only new infection times  $t_j^I$  are observed, the new recovery times  $t_j^R$  are unobserved. **(middle panel)** The corresponding size of the infectious population  $I(t)$  over time. **(lower panel)** The new infection rate  $\lambda^I(t)$  and the new recovery rate  $\lambda^R(t)$ . SIR parameters:  $N = 5$ ,  $\beta = 2$ ,  $\gamma = 0.5$ .

over all times to recovery  $\tau$  is equal to the expectation of  $\lambda^H(t)$  over individual event strengths  $m$ .

$$\mathbb{E}_\tau[\lambda^I(t)] = \mathbb{E}_m[\lambda^H(t)],$$

when  $\mu(t) = 0$ ,  $\beta = \kappa\theta \frac{\alpha-1}{\alpha-\eta-1}$ ,  $\gamma = \theta$ .

The rest of this section proves this theorem.

**Stochastic SIR as a bivariate Poisson process.** One classic view of the SIR model is that of a bivariate continuous time-homogeneous Markov chain  $\{S(t), I(t)\}$  [2].  $S(t), I(t) : \mathbb{R} \rightarrow \mathbb{N}$  are random functions that uniquely define the state of the process, since  $R(t) = N - S(t) - I(t)$  for a fixed population. Given the state  $\{S(t) = s, I(t) = i\}$ , in the infinitesimal interval  $\delta t$ , chosen small enough to guarantee that at most one event occurs between  $t$  and  $t + \delta t$ , one of the following three options can happen a new infection occurs and the system transitions to the state  $\{S(t + \delta t) = s - 1, I(t + \delta t) = i + 1\}$ ; a new recovery occurs and the system transitions to the state  $\{S(t + \delta t) = s, I(t + \delta t) = i - 1\}$ ; or none of the above happen and the system remains in the state  $\{S(t + \delta t) = s, I(t + \delta t) = i\}$ .

The SIR process can be represented as a bivariate point process, in which two types of events occur: *infection events* and *recovery events* [39]. The  $j$ -th infected individual in the SIR process gets infected at time  $t_j^I$  and recovers at time  $t_j^R$ . Her time to recovery is defined as:  $\tau_j = t_j^R - t_j^I$ . Let  $C_t$  be the counting process of the infection process and  $R_t$  the counting process of the recovery process. Given  $\mathcal{H}_t$  – the history of the epidemic process up to time  $t$  – and under the time stationary Markov chain assumption, it can be

shown that:

$$\begin{aligned} \mathbb{P}(C_{t+\delta t} - C_t = 1 | \mathcal{H}_t) &\approx \beta \frac{S(t)}{N} I(t) \delta t \\ \mathbb{P}(C_{t+\delta t} - C_t > 1 | \mathcal{H}_t) &= 0 \\ \mathbb{P}(C_{t+\delta t} - C_t = 0 | \mathcal{H}_t) &\approx 1 - \beta \frac{S(t)}{N} I(t) \delta t. \end{aligned} \quad (12)$$

A similar result can be shown for the recovery process  $R_t$ . Given Eq. (12) and the definition of a non-homogeneous Poisson process (Eq. (1)), the following holds:

**LEMMA 3.2.** *An SIR process can be formulated as a bivariate non-homogeneous Poisson process, in which the new infection rate  $\lambda^I(t)$  and the new recovery rate  $\lambda^R(t)$  are:*

$$\lambda^I(t) = \beta \frac{S(t)}{N} I(t); \quad \lambda^R(t) = \gamma I(t).$$

Fig. 2 illustrates an SIR as a bivariate Poisson process: five infection events occur at times  $t_1^I, \dots, t_5^I$  (shown in red); five recovery events occur at  $t_1^R, \dots, t_5^R$  (shown in blue). To each infection event corresponds a recovery event. The middle panel of Fig. 2 show the size of the infected population  $I(t)$  over time. Each new infection event increments  $I(t)$ , and each new recovery decreases  $I(t)$  by one. The bottom panel of Fig. 2 shows the new infection and new recovery rates for the SIR process with five individuals. Initially,  $\lambda^I(t)$  is significantly higher than  $\lambda^R(t)$ . As the number of susceptible individuals  $S(t)$  gets depleted, the  $\frac{S(t)}{N}$  term inhibits  $\lambda^I(t)$  which becomes zero after the fifth infection ( $S(t) = 0, t \geq t_5^I$ ). The new recovery rate also becomes zero after the last infected individual recovers ( $I(t) = 0, t \geq t_5^R$ ).

**The expected new infections rate.**  $S(t)$  and  $I(t)$  in Lemma 3.2 are random functions of the infection and recovery processes, alternatively expressed with indicator functions on the event times.

$$\begin{aligned} S(t) &= N - C_t = N - \sum_{j \geq 1} \mathbb{1}(t_j^I < t) \\ I(t) &= C_t - R_t = \sum_{j \geq 1} \mathbb{1}(t_j^I < t, t_j^R > t) = \sum_{t_j^I < t} \mathbb{1}(t_j^I + \tau_j > t). \end{aligned} \quad (13)$$

We examine a point process consisting only of the infection events  $\{t_j^I\}$ . The event rate in this process is obtained by marginalising out times of recovery  $\mathbb{E}_\tau[\lambda^I(t)]$ .

$$\begin{aligned} \mathbb{E}_\tau[\lambda^I(t)] &\stackrel{Lm. 3.2}{=} \mathbb{E}_\tau \left[ \beta \frac{S(t)}{N} \sum_{t_j^I < t} \mathbb{1}(t_j^I + \tau_j > t) \right] \\ &= \sum_{t_j^I < t} \mathbb{E}_\tau \left[ \beta \frac{S(t)}{N} \mathbb{1}(t_j^I + \tau_j > t) \right] \\ &= \sum_{t_j^I < t} \int_0^\infty \beta \frac{S(t)}{N} \mathbb{1}(t_j^I + \tau > t) r(\tau) d\tau \\ &= \sum_{t_j^I < t} \beta \frac{S(t)}{N} \int_{t-t_j^I}^\infty r(\tau) d\tau, \end{aligned} \quad (14)$$

where  $r(\tau)$  is the exponential probability distribution function for the time to recovery (cf. Sec. 3.1). Knowing  $S(t) = N - C_t$ , we obtain:

$$\mathbb{E}_\tau \left[ \lambda^I(t) \right] = \left( 1 - \frac{C_t}{N} \right) \sum_{t_j^I < t} \beta e^{-\gamma(t-t_j^I)} \quad (15)$$

**Expected event rate in HawkesN over user influence.** In the stochastic SIR model, the actions of each individual are guided by the same set of global rules, i.e. the differences between individuals are not observed. The HawkesN model with the kernel defined in Eq. (4) accounts for different local user influences, which are averaged out in Theorem 3.1. We obtain:

$$\begin{aligned} \mathbb{E}_m \left[ \lambda^H(t) \right] &= \mathbb{E}_m \left[ \left( 1 - \frac{N_t}{N} \right) \left( \mu(t) + \sum_{t_j < t} \kappa m_j^\eta \theta e^{-\theta(t-t_j)} \right) \right] \\ &= \left( 1 - \frac{N_t}{N} \right) \left( \mu(t) + \sum_{t_j < t} \kappa \theta e^{-\theta(t-t_j)} \int_1^\infty m^\eta p(m) dm \right) \\ &= \left( 1 - \frac{N_t}{N} \right) \left( \mu(t) + \sum_{t_j < t} K \theta e^{-\theta(t-t_j)} \right) \end{aligned} \quad (16)$$

Where  $p(m)$  is the distribution of local user influence of parameter  $\alpha$  (see Sec. 2.2). As a result,  $K$  in Eq. (16) is  $K = \kappa \frac{\alpha-1}{\alpha-\eta-1}$ .

We can see that Eq. (15) and (16) are identical when  $N_t = C_t$  (i.e. we observed the same random process) and under the parameter equivalence in Theorem 3.1. That is to say, the new infection point process in an SIR model is equivalent in expectation with a HawkesN point-process with no background event rate. This completes the proof of Theorem 3.1. We also demonstrate the equivalence empirically, through simulation and subsequent parameter fitting, in the online supplement [1].

### 3.3 Derived properties

**COROLLARY 3.3.** *The Basic Reproduction Number of an SIR process and the branching factor of its equivalent HawkesN process (according to Theorem 3.1) are equal.*

$$\text{Proof: } n^* \stackrel{\text{Eq. (5)}}{=} \kappa \frac{\alpha-1}{\alpha-\eta-1} \stackrel{\text{Th. 3.1}}{=} \frac{\beta}{\gamma} = \mathcal{R}_0.$$

Corollary 3.3 is significant because it links two of the most important quantities in the HawkesN and the SIR models, which have been used to address apparently unrelated problems. For example, the branching factor  $n^*$  has been used as a threshold in seismology to differentiate between aftershock behavior [17, 18], in social media analysis to predict information cascade sizes [23, 44] and to predict the virality and promotion potential of online content [28, 29]. The basic reproduction number  $\mathcal{R}_0$  has been used in epidemiology to quantify the probability of disease extinction, the final size distribution, and expected duration of an epidemic [2, 39] and in social media to measure the “quality” of retweet cascades [22]. The link shown in this section allows to bring mature techniques employed with SIR into the world of online diffusion modeling with Hawkes processes.

## 4 DIFFUSION SIZE DISTRIBUTION

We compute the distribution of the final size of an information diffusion cascade which has been partially observed and fitted using

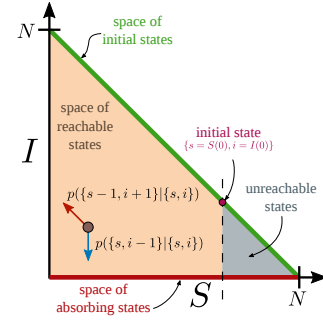


**Figure 3: Visualization of the space of states of the SIR bivariate Markov Chain  $\{s, i\}$ .**  $s, i \in \mathbb{N}$  and  $s + i \leq N$ , in other words the space of valid states sits under the green line  $s + i = N$ . The initial state in an SIR epidemic is always on the green line ( $S(0) + I(0) = N$ ). Given an initial state  $\{s = S(0), i = I(0)\}$  (shown by the magenta circle), the orange area shows the space of reachable states and the gray area depicts the unreachable states. From a state  $\{s, i\}$  the system can to  $\{s-1, i+1\}$  (new infection); and to  $\{s, i-1\}$  (new recovery). The absorbing states ( $\{s, 0\}$ ) is shown with a red line.

HawkesN, using a Markov chain technique developed for SIR. In Sec. 4.1 we review known results on the final size distribution of an SIR epidemic. In Sec. 4.2 we employ the equivalence shown in Theorem 3.1 to compute the final size distribution of a cascade modeled with HawkesN.

### 4.1 Epidemic size distributions in SIR

The final size of an infection is defined as the total number of individuals that have been infected (and recovered) during the epidemic. Estimating the final size while the epidemics in the early stages is a well-studied problem in epidemiology. In this section, we review solutions to this problem for the deterministic SIR model and the stochastic SIR model introduced in Sec. 3.1.

**Final Size in the Deterministic SIR.** Computing the final size in the deterministic model is straightforward, as it results directly from the differential equations in Eq. (8)-(10). Allen [2] shows that dividing Eq. (9) by Eq. (8) and integrating, we obtain:

$$\begin{aligned} \Rightarrow \frac{dI}{dS} &= -1 + \frac{N\gamma}{\beta S} \\ \Rightarrow I(t) + S(t) &= I(0) + S(0) + \frac{N\gamma}{\beta} \log \frac{S(t)}{S(0)} \\ t \rightarrow \infty, I(\infty) &= 0 \Rightarrow S(\infty) = N + \frac{N\gamma}{\beta} \log \frac{S(\infty)}{S(0)}. \end{aligned} \quad (17)$$

Eq (17) has a root in  $[0, N]$ , which we find numerically. The prediction of final size for the deterministic SIR is  $R(\infty) = N - S(\infty)$ .

**Distribution of final size in the stochastic SIR.** We represent the stochastic SIR process using the bivariate continuous-time Markov chain formulation presented in Sec. 3.2. Each state is uniquely defined by the ordered pair  $\{s, i\}$ , denoting the sizes of the susceptible and infected populations. The space of states  $\Sigma$  is visually represented in Fig. 3 as a triangle on the two-dimensional



surface  $S - I$ . From in a given state  $\{s, i\}$ , there are only two possible outcomes: a new infection arrives, and the system transitions  $\{s, i\} \rightarrow \{s - 1, i + 1\}$  with the probability  $p(\{s - 1, i + 1\}|\{s, i\})$ ; or a new recovery arrives, and the system transitions  $\{s, i\} \rightarrow \{s, i - 1\}$  with the probability  $p(\{s, i - 1\}|\{s, i\})$  (shown in the figure by the red and blue arrows, respectively). The epidemic ends when  $I(t)$  reaches zero, i.e. the states  $\{s, 0\}$  are absorbing – *once the system arrives in one of these states, it does not transition to any other state*. From an initial point  $\{S(0), I(0)\}$  the system can finish in any of the absorbing states  $\{s, 0\}$  with the probability  $P(s)$ , where  $s = 0, \dots, N - I(0)$ . The distribution of final size is simply  $P(N - s)$ .

**Transition matrix and state probabilities.** When in the state  $\{s, i\}$ , the rate of new infections is  $\frac{\beta}{N}si$  and the rate of new recoveries is  $\gamma i$ . Knowing that  $p(\{s - 1, i + 1\}|\{s, i\}) + p(\{s, i - 1\}|\{s, i\}) = 1$ , we compute:

$$\begin{aligned} p(\{s - 1, i + 1\}|\{s, i\}) &= \frac{\frac{\beta}{N}si}{\frac{\beta}{N}si + \gamma i} = \frac{\beta s}{\beta s + N\gamma} \\ p(\{s, i - 1\}|\{s, i\}) &= \frac{\gamma i}{\frac{\beta}{N}si + \gamma i} = \frac{N\gamma}{\beta s + N\gamma}. \end{aligned} \quad (18)$$

This is of course true unless  $\{s, i\}$  is an absorbing state, in which case  $p(\{s, i\}|\{s, i\}) = 1$  and the probability for any other transition is zero. We denote by  $\sigma = \{s, i\}$  a state in the space of states  $\Sigma$ . We use Eq. (18) to compute the transition matrix  $T$  of size  $|\Sigma| \times |\Sigma|$ , where  $T_{i,j}$  is the probability of transitioning from state  $\sigma_j$  to state  $\sigma_i$ . Given  $p$  be a vector of size  $|\Sigma|$ , with  $p_j$  being the probability of being in the state  $\sigma_j$  at a given moment, the probability distribution over the states after the next event is  $p' = T \times p$ . Starting from  $p = [0, \dots, 0, 1, 0, \dots, 0]$ , where the 1 corresponds to the initial state  $\sigma_0 = \{S(0), I(0)\}$ , we obtain the final distribution over states by running the simulation forward  $2N - 1$  steps, after which it is guaranteed to converge [2]. At convergence, all states except the absorbing states have a probability of zero.

## 4.2 Cascade size distribution in HawkesN

For a HawkesN model of given parameters, we can obtain the probability distribution of its final size by obtaining the equivalent SIR model (using Theorem 3.1) and applying the method described in the previous section. This is the *a priori* probability distribution at time  $t = 0$  – after observing the first event. If we have observed instead  $l$  events, we can compute the *a posteriori* probability distribution accounting for the observed events. We run forward the simulation algorithm described in Sec. 4 from the initial state  $\{S(t_l), I(t_l)\}$ . Because recovery events are not observed in HawkesN, the exact size of the infected population is not known. We use instead the expected size of the infected population at time  $t_l$ :

$$\mathbb{E}_\tau[I(t_l)] = \mathbb{E}_\tau \left[ \sum_{j=1}^l \mathbb{1}(t_j^I + \tau_j > t_l) \right] \stackrel{\text{Eq. (14), (15)}}{=} \sum_{j=1}^l e^{-\gamma(t_l - t_j^I)}$$

In our experiments in Sec. 5.5, we compute the *a posteriori* probability distribution by simulating forward the Markov chain from the state  $\sigma_0 = \{N - l, \mathbb{E}_\tau[I(t_l)]\}$ .

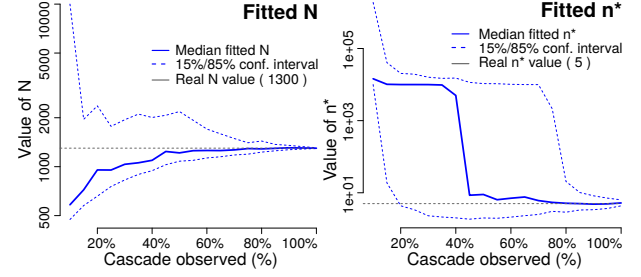


**Figure 4: Robustness of estimating the population size  $N$  and the branching factor  $n^*$  for HawkesN.** One set of parameters for each model was simulated 100 times and fitted on increasingly longer prefixes of each simulation. One value for  $N$  and  $n^*$  is obtained for each fit and the median and the 15%/85% percentile values are shown.

## 5 EXPERIMENTS AND RESULTS

In this section, we investigate the performances of HawkesN. First in Sec 5.1 we investigate on synthetic data the number of observations required to fit a HawkesN model. We then evaluate HawkesN on three diffusion datasets on Twitter. Sec. 5.2 describes the datasets. Sec. 5.3 evaluates the generalization performance of HawkesN. Sec. 5.4 analyzes the branching factor across different datasets. Sec. 5.5 profiles cascade size distributions, and has a new explanation for the perceived popularity unpredictability.

### 5.1 Robustness of fit for HawkesN

One key question regarding the HawkesN process in the context of modeling information diffusion is the number of events in each cascade that need to be observed for an accurate estimation of the parameters. This is particularly important when the maximum number of events  $N$  is not known in advance and needs to be estimated from data. Starting from a set of parameters, we simulate 100 realizations. We fit HawkesN on increasing prefixes of each realization. Fig. 4 shows the graphics for the branching factor and parameter  $N$  for HawkesN (the graphics for the other parameters are shown in the online supplement [1]). For calibration, we perform the same exercise for the basic Hawkes Process and we presents the graphic for its branching factor in Fig. 10a. We chose to show these parameters as they are highly indicative for the unfolding of the rest of the cascade (as shown in Sec. 4). The basic Hawkes requires observing less the 30% of the length of the cascade to make reliable estimates. Our proposed HawkesN model is more sensitive to the amount of available information, and requires observing more than 40% of the cascade before the median  $n^*$  and  $N$  estimates approach the true values. This is because we estimate the population size  $N$  from observed data. Alternatively,  $N$  could be estimated from past diffusions (discussed in Sec. 7).

### 5.2 Datasets

We use three datasets of retweet diffusion cascades in Twitter, used in previous work. For each tweet in each cascade, we have information about the time offset of the retweet and the number of followers of the user posting the retweet. The ACTIVE dataset was collected by Rizoio et al. [29] during 6 months in 2014. It contains

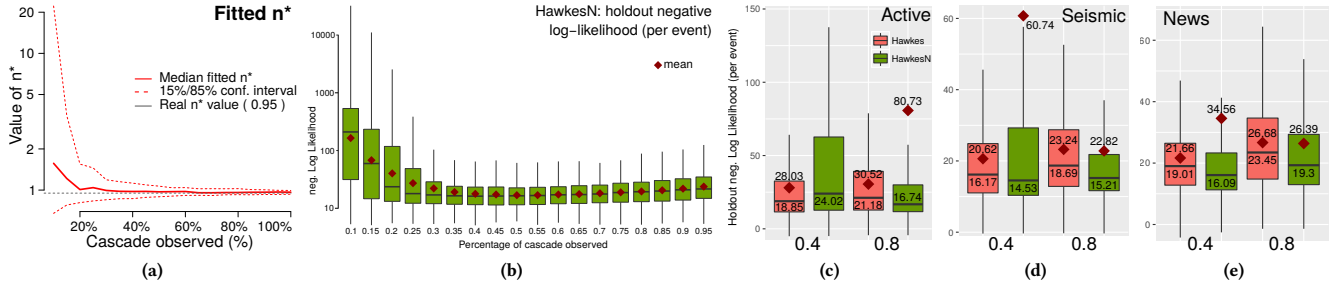


Figure 5: (a) Reliability of fit for the basic Hawkes model. (b)-(e) Performances of HawkesN explaining unobserved data, using holdout negative log likelihood. The performance over all cascades in a dataset are summarized using boxplots, lower is better (b). The percentage of observed events in each cascade used to train HawkesN is varied between 10% and 95%. We use 1000 cascades randomly sampled from NEWS. (c), (d) and (e) The performances on all cascades of ACTIVE, SEISMIC and NEWS, for Hawkes and HawkesN, when observing 40% and 80% of each cascade.

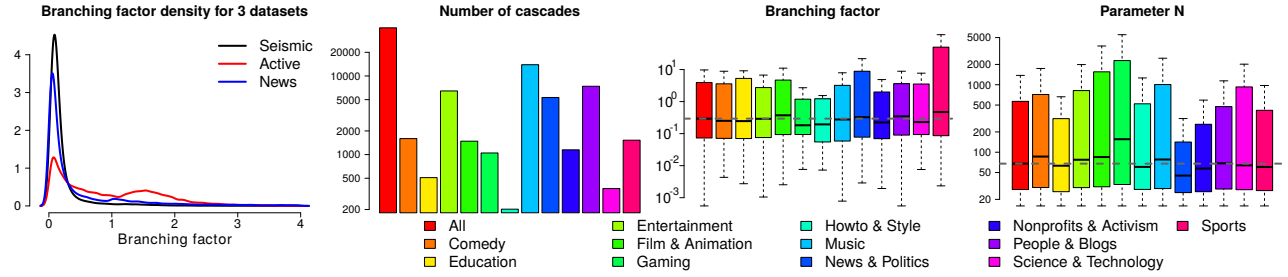


Figure 6: (first panel) Density distribution for the branching factor of HawkesN, for the three studied datasets (only  $n^* \leq 4$  is showed here). (last three panels) The number of cascades associated with Youtube videos in the ACTIVE dataset, the branching factor  $n^*$  and population size  $N$  (fitted by HawkesN), tabulated against video category.

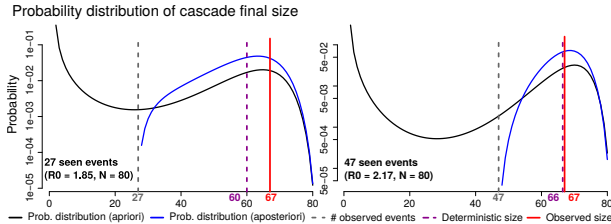


Figure 7: Final size probability distribution for a NEWS cascade. HawkesN was fitted on the first 27 events (left) and 47 events (right). The black line shows the *apriori* distribution, before seeing any events. the blue line shows the *aposteriori* distribution, after seeing the observed events. Shown with vertical lines: the number of observed events in gray dashed, the deterministic prediction in magenta dashed and the actual observed cascade size in red.

Table 1: Datasets profiling: number of cascades and number of tweets; min, mean and median cascade size.

	#cascades	#tweets	Min.	Mean	Median
ACTIVE [29]	41,411	8,142,892	20	197	41
SEISMIC [44]	166,076	34,784,488	50	209	111
NEWS [23]	20,093	3,252,549	50	162	90

more than 41k retweet cascades related to more than 13k Youtube videos, each cascade containing at least 20 tweets. Each Youtube video has assigned a category – such as Music, Gaming or Film & Animation –, that we make use of in Sec. 5.4. The SEISMIC dataset was collected by Zhao et al. [44]. It contains a sample of all tweets during a month (i.e. using the firehose Twitter API restricted access), further filtered so that the length of each cascade is greater than 50. The NEWS dataset was collected by Mishra et al. [23] over a period of four months in 2015. They selected tweets containing links to news articles, by tracking the official twitter handles of popular news outlets, such as NewYork Times, or CNN. Each cascade contains at least 50 tweets. Table 1 summarizes these datasets.

### 5.3 Generalization to unobserved data

**Setup.** We empirically validate the fitness of HawkesN by studying how it generalizes to unseen data. We adopt the setup in [3, 9, 12, 29, 30, 44]: a diffusion is partially observed, i.e. HawkesN observes a set of  $l$  events  $\{m_j, t_j\}, t = 1, \dots, l$ , and we measure the holdout likelihood, i.e. the likelihood of the events in the unobserved period (events  $\{m_j, t_j\}, t = l + 1, \dots, n$ ), using Eq. 6. The higher the holdout likelihood, the better the model generalizes to unseen data. We report the average holdout likelihood per event, to render the results comparable across holdout sets containing different numbers of events. Given the results in Sec. 5.1, concerning the length of observed data required to make reliable estimates, we



chose to observe in each cascade a given percentage of all events, to render the results comparable across cascades of different length. We compare HawkesN with the state-of-the-art Hawkes model for information diffusion, proposed by Mishra et al. [23].

**Results.** Fig. 10b shows the generalization performances of HawkesN, when varying the percentage of observed events from 10% to 95%. Consistent with the results on the synthetic data in Sec. 5.1, we observe a high variance of performance when observing less than 40% of each cascade. The basic Hawkes model shows less variance at lower percentages (shown in the online supplement [1]). Plots (c) to (e) in Fig. 5 show the generalization performance of Hawkes and HawkesN, on the three datasets, for the observed percentages of 40% and 80%. Visibly, HawkesN consistently outperforms the basic Hawkes. For both models, the generalization appears to slightly worsen for higher percentages, due to overfitting. In conclusion, the HawkesN model has a higher explanatory power for unobserved data, however it requires more training data when the population size  $N$  also needs to be estimated.

## 5.4 Branching factor

Here we study the branching factor  $n^*$ . We fit HawkesN by observing 80% of each cascade, and we compute  $n^*$  using Eq. 5. Fig. 6 (left) shows the density distribution of  $n^*$  in the three datasets. For SEISMIC and NEWS, there is a peak around 0.2, followed by a long tail. This is consistent with the findings of Martin et al. [22]. For ACTIVE however, the density shows a secondary peak around 1.5, which is probably related to the fact that this dataset contains diffusion about Youtube videos. We further investigate  $n^*$  on ACTIVE, by tabulating cascades against the category of the video that the cascade relates to. Notably, cascades related to Sports, People & Blogs and Film & Animation tend to have higher values of  $n^*$  than the dataset median. Similarly, cascade in Gaming, Howto & Style and Nonprofit & Activism have lower  $n^*$ . When studying the population size  $N$ , Gaming stands out as particular category as it has relative high values of  $N$ . This is indicative of a large user reach for information relating to Gaming diffusions.

## 5.5 Explaining popularity unpredictability

In this section, we study the probability distribution of size for real-life cascades. For lower values of  $n^*$ , the the probability distribution for the cascade size is skewed towards lower cascade sizes. Similarly, for high values of  $n^*$  it is skewed towards the maximum population size  $N$  [2]. In Fig. 7 we chose a cascade from the NEWS dataset with  $n^* \approx 2$ , because this value shows borderline behavior, and because of the secondary density maximum in Fig. 6. Both left and right plots in Fig. 7 show the same cascade, with the HawkesN parameters fit on 27 and 47 events respectively ( $n = 80$ ). The *a priori* probability size distribution – the distribution after observing only the first event – shows two maxima: one around very small values of cascade size, and one around  $\sim 65$ . This provides the following explanation for the general perceived unpredictability of online popularity. A cascade of a given “potential”  $n^*$  [22] can achieve any size with a given probability and for  $n^* \sim 2$  there are two likely outcomes: either it dies out early or it reaches a large size compared to the maximum population  $N$ . At time  $t = 0$  is it impossible to differentiate between the two outcomes. The situation is different

after observing a number of events. The *aposteriori* probability distribution (shown in Fig. 7 with a blue line) reflects the information gained from the observed events and it shows a single maximum towards the higher size values. The more events we observe, the higher the likelihood of the observed cascade size. This provides another explanation to why autoregressive popularity prediction approaches [6, 27, 32] achieve higher results. The unpredictability of popularity has been previously theorized [22], however as far as we know this is the first theoretically-grounded proof for it.

## 6 RELATED WORK

We structure related work into two broad categories, based on the used framework: point process approaches and epidemic models.

**Point process approaches.** Popularity modeling [7, 9, 40] and prediction [29, 30, 44] has been a particularly fertile field for point-process based generative models. In their seminal work, Crane and Sornette [7] showed how a Hawkes point-process can account for popularity bursts and decays. More sophisticated models have been proposed to model and simulate popularity in microblogs [40] and videos [9]. These approaches successfully account for the social phenomena which modulate online diffusion: the “rich-get-richer” phenomenon and social contagion. Certain models can output an estimate for the total size of a retweet cascade. Shen et al. [30] employ reinforced Poisson processes, modeling three phenomena: fitness of an item, a temporal relaxation function and a reinforcement mechanism; while SEISMIC [44] employs a double stochastic process, one accounting for infectiousness and the other one for the arrival time of events. Our work differs from the above in two aspects. First it proposes a generalization of the Hawkes model, which operates in a finite population – which is a more realistic assumption. Second, it outputs a size probability distribution and it explains the perceived unpredictability of online popularity [22].

A recently emerging body of work employs Stochastic Differential Equations to formulate Hawkes point processes. RedQueen [43] and Cheshire [42] are two algorithms aimed at optimizing social influence, which they formulate as a stochastic optimal control problem. Wang et al. [36] use stochastic control and reinforcement learning to address the user activity guiding problem and feedback in social systems. Later, Wang et al. [37] use the stochastic differential equation model to link the microscopic event data and macroscopic inference, and to approximate its probability distribution. The similarity between the above and our work is at the level of tools, by using stochastic calculus to link the event-level to the event rate and compute expected quantities. However, none of the above links point processes to epidemic models. The advantage of our solution is that it enables to leverage the mature tools in epidemic models to the field of information diffusion.

**Epidemic model approaches.** Despite being developed for the field of epidemiology, epidemic models have been applied to information diffusion problems through the analogy of information spread as a disease. Classic epidemic models were early applied in the knowledge and scientific theory diffusion study [13] and latter employed in many areas, such as economic and finance time series analysis [31]. Pastor-Satorras and Vespignani [25] applied SIS (Susceptible-Infected-Susceptible) epidemic model to simulate computer virus transmission over the Internet. A series of studies

analyzed the spread of rumors in complex networks based on an epidemic model [24, 33, 41]. More recently, Woo and Chen [38] modeled topic diffusion in web forums using an SIR model; Martin et al. [22] fitted an epidemic model to retweet cascades and used the computed basic reproduction number to theorize the unpredictability of online popularity. However these work do not leverage tools specific to epidemic models (such as computing the probability distribution of size), nor do they link to point process models as our work does.

## 7 DISCUSSION

In this work, we present a previously unexplored connection between Hawkes point processes and SIR epidemic models. First we propose HawkesN, an extension of the Hawkes process with a finite number of events. Next we consider that events in Hawkes correspond to new infections in SIR, and we show that the two processes are equivalent in expectation. This paves the way to applying tools developed for one approach, across the gap, to the other approach. We present a novel method to compute the probability distribution of final size of a cascade after observing its initial unfolding using HawkesN, which is based on a Markov chain tool developed for SIR. We use the probability of cascade size on a large sample of real cascades to provide a nuanced explanation for the general unpredictability of popularity.

**Assumptions, limitations and future work.** This work assumes a fixed population (users don't enter, nor do they exit). A link could be drawn between evolving populations in SIR and  $\mu(t) \neq 0$  in HawkesN. The current work assumes that the maximum population size  $N$  is estimated for each cascade, while observing it. Future work could use other observed similar cascades to infer the size of a "thematic neighborhood" before a cascade starts unfolding. Finally, allowing for user-specific behavior in the SIR model or kernel functions other than the exponential function requires more advanced SIR formulations, such as an agent-based formulation.

## REFERENCES

- [1] 2017. Appendix: SIR Hawkes: Linking Epidemic Models and Hawkes Point Processes for Online Information Diffusion. (2017). <https://www.dropbox.com/s/506aifouevua1n/WWW-2018-SI.pdf?dl=0>.
- [2] Linda J. S. Allen. 2008. An Introduction to Stochastic Epidemic Models. In *Mathematical Epidemiology*. Springer, Berlin, Heidelberg, Chapter 3, 81–130. [https://doi.org/10.1007/978-3-540-78911-6\\_3](https://doi.org/10.1007/978-3-540-78911-6_3)
- [3] Peng Bao, Hua-Wei Shen, Xiaolong Jin, and Xue-Qi Cheng. 2015. Modeling and Predicting Popularity Dynamics of Microblogs using Self-Excited Hawkes Processes. In *Proceedings of the 24th International Conference on World Wide Web - WWW '15 Companion*. ACM Press, New York, New York, USA, 9–10. <https://doi.org/10.1145/2740908.2742744>
- [4] Georgiy V. Bobashev, D. Michael Goedecke, Feng Yu, and Joshua M. Epstein. 2007. A hybrid epidemic model: Combining the advantages of agent-based and equation-based approaches. In *Proceedings - Winter Simulation Conference*. IEEE, 1532–1537. <https://doi.org/10.1109/WSC.2007.4419767>
- [5] Tom Britton. 2010. Stochastic epidemic models: A survey. *Mathematical Biosciences* 225, 1 (may 2010), 24–35. <https://doi.org/10.1016/j.mbs.2010.01.006>
- [6] Biao Chang, Hengshu Zhu, Yong Ge, Enhong Chen, Hui Xiong, and Chang Tan. 2014. Predicting the Popularity of Online Serials with Autoregressive Models. In *Proceedings of the 23rd ACM International Conference on Conference on Information and Knowledge Management - CIKM '14*. ACM Press, New York, New York, USA, 1339–1348. <https://doi.org/10.1145/2661829.2662055>
- [7] Riley Crane and Didier Sornette. 2008. Robust dynamic classes revealed by measuring the response function of a social system. *Proceedings of the National Academy of Sciences* 105, 41 (oct 2008), 15649–15653. <https://doi.org/10.1073/pnas.0803685105>
- [8] D J Daley and D Vere-Jones. 2008. *An introduction to the theory of point processes. [V]ol. [I].* Vol. I. xviii+573 pages. <https://doi.org/10.1007/b97277>
- [9] Wanying Ding, Yue Shang, Lifan Guo, Xiaohua Hu, Rui Yan, and Tingting He. 2015. Video Popularity Prediction by Sentiment Propagation via Implicit Network. In *Proceedings of the 24th ACM International Conference on Information and Knowledge Management*. ACM, 1621–1630. <https://doi.org/10.1145/2806416.2806505>
- [10] Robert Fourer, David M Gay, and Brian Kernighan. 1993. *AMPL*. Vol. 117. Boyd & Fraser Danvers, MA.
- [11] Robert Fourer, David M Gay, and Brian W Kernighan. 1987. *AMPL: A mathematical programming language*. AT&T Bell Laboratories Murray Hill, NJ 07974.
- [12] Shuai Gao, Jun Ma, and Zhumin Chen. 2015. Modeling and Predicting Retweeting Dynamics on Microblogging Platforms. In *Proceedings of the Eighth ACM International Conference on Web Search and Data Mining - WSDM '15*. ACM Press, New York, New York, USA, 107–116. <https://doi.org/10.1145/2684822.2685303>
- [13] William Goffman. 1971. A Mathematical Method for Analyzing the Growth of a Scientific Discipline. *Journal of the ACM (JACM)* 18, 2 (apr 1971), 173–185. <https://doi.org/10.1145/321637.321640>
- [14] Jacob Goldenberg, Barak Libai, and Eitan Muller. 2001. Talk of the Network: A Complex Systems Look at the Underlying Process of Word-of-Mouth. *Marketing Letters* 12 (2001), 211–223. <https://doi.org/10.1023/A:1011122126881>
- [15] Manuel Gomez-Rodriguez, Le Song, Nan Du, Hongyuan Zha, and Bernhard Schölkopf. 2016. Influence Estimation and Maximization in Continuous-Time Diffusion Networks. *ACM Transactions on Information Systems* 34, 2 (feb 2016), 1–33. <https://doi.org/10.1145/2824253>
- [16] Alan G. Hawkes. 1971. Spectra of some self-exciting and mutually exciting point processes. *Biometrika* 58, 1 (apr 1971), 83–90. <https://doi.org/10.1093/biomet/58.1.83>
- [17] Agnès Helmstetter and Didier Sornette. 2002. Subcritical and supercritical regimes in epidemic models of earthquake aftershocks. *Journal of Geophysical Research: Solid Earth* 107, B10 (2002), ESE 10–1—ESE 10–21. <https://doi.org/10.1029/2001jb001580> arXiv:cond-mat/0109318
- [18] Y. Y. Kagan. 1991. Likelihood analysis of earthquake catalogues. *Geophysical Journal International* 106, 1 (jul 1991), 135–148. <https://doi.org/10.1111/j.1365-246X.1991.tb04607.x>
- [19] W. O. Kermack and A. G. McKendrick. 1927. A Contribution to the Mathematical Theory of Epidemics. *Proceedings of the Royal Society A: Mathematical, Physical and Engineering Sciences* 115, 772 (aug 1927), 700–721. <https://doi.org/10.1098/rspa.1927.0118>
- [20] Ryota Kobayashi and Renaud Lambiotte. 2016. TiDeH: Time-Dependent Hawkes Process for Predicting Retweet Dynamics. In *ICWSM 2016*. arXiv:1603.09449
- [21] Dong C. Liu and Jorge Nocedal. 1989. On the limited memory BFGS method for large scale optimization. *Mathematical Programming* 45, 1-3 (aug 1989), 503–528. <https://doi.org/10.1007/BF01589116>
- [22] Travis Martin, Jake M. Hofman, Amit Sharma, Ashton Anderson, and Duncan J. Watts. 2016. Exploring Limits to Prediction in Complex Social Systems. In *Proceedings of the 25th International Conference on World Wide Web*. 683–694. <https://doi.org/10.1145/2872427.2883001> arXiv:1602.01013
- [23] Swapnil Mishra, Marian-Andrei Rizoiu, and Lexing Xie. 2016. Feature Driven and Point Process Approaches for Popularity Prediction. In *Proceedings of the 25th ACM International Conference on Information and Knowledge Management - CIKM '16*. ACM Press, Indianapolis, IN, USA, 1069–1078. <https://doi.org/10.1145/2983323.2983812>
- [24] Yamin Moreno, Maziar Nekovee, and Amalio F. Pacheco. 2004. Dynamics of rumor spreading in complex networks. *Physical Review E - Statistical, Nonlinear, and Soft Matter Physics* 69, 6 2 (jun 2004), 066130. <https://doi.org/10.1103/PhysRevE.69.066130> arXiv:cond-mat/0312131
- [25] Romualdo Pastor-Satorras and Alessandro Vespignani. 2001. Epidemic spreading in scale-free networks. *Physical Review Letters* 86, 14 (apr 2001), 3200–3203. <https://doi.org/10.1103/PhysRevLett.86.3200> arXiv:cond-mat/0010317
- [26] János D Pintér. 1997. LGO-A program system for continuous and Lipschitz global optimization. *Nonconvex Optimization and Its Applications* 18 (1997), 183–198.
- [27] Henrique Pinto, Jussara M. Almeida, and Marcos A. Gonçalves. 2013. Using early view patterns to predict the popularity of youtube videos. In *Proceedings of the sixth ACM international conference on Web search and data mining - WSDM '13*. ACM Press, New York, New York, USA, 365. <https://doi.org/10.1145/2433396.2433443>
- [28] Marian-Andrei Rizoiu and Lexing Xie. 2017. Online Popularity under Promotion: Viral Potential, Forecasting, and the Economics of Time. In *11th International AAAI Conference on Web and Social Media - ICWSM'17*. 182–191. <https://aaai.org/ocs/index.php/ICWSM/ICWSM17/paper/view/15553>
- [29] Marian-Andrei Rizoiu, Lexing Xie, Scott Sanner, Manuel Cebrian, Honglin Yu, and Pascal Van Hentenryck. 2017. Expecting to be HIP: Hawkes Intensity Processes for Social Media Popularity. In *26th International Conference on World Wide Web - WWW '17*. ACM Press, Perth, Australia, 735–744. <https://doi.org/10.1145/3038912.3052650> arXiv:1602.06033
- [30] Hw Shen, Dashun Wang, Chaoming Song, and Al Barabási. 2014. Modeling and Predicting Popularity Dynamics via Reinforced Poisson Processes. In *Proceedings of the Twenty-Eighth AAAI Conference on Artificial Intelligence*. AAAI Press, Québec City, Québec, Canada, 291–297. arXiv:arXiv:1401.0778v1

- [31] Ernest S. Shtatland and Timur Shtatland. 2008. Another Look at Low-Order Autoregressive Models in Early Detection of Epidemic Outbreaks and Explosive Behaviors in Economic and Financial Time Series. In *SGF Proceedings*. Cary, NC: SAS Institute, Inc.
- [32] Gabor Szabo and Bernardo a. Huberman. 2010. Predicting the popularity of online content. *Commun. ACM* 53, 8 (aug 2010), 80. <https://doi.org/10.1145/1787234.1787254> arXiv:0811.0405
- [33] Daniel Trpevski, Wallace K. S. Tang, and Ljupco Kocarev. 2010. Model for rumor spreading over networks. *Physical Review E - Statistical, Nonlinear, and Soft Matter Physics* 81, 5 (may 2010), 056102. <https://doi.org/10.1103/PhysRevE.81.056102>
- [34] A Wächter and L T Biegler. 2006. On the Implementation of a Primal-Dual Interior Point Filter Line Search Algorithm for Large-Scale Nonlinear Programming. *Mathematical Programming* 106, 1 (2006), 25–57.
- [35] Jacco Wallinga and Peter Teunis. 2004. Different epidemic curves for severe acute respiratory syndrome reveal similar impacts of control measures. *American journal of epidemiology* 160, 6 (sep 2004), 509–16. <https://doi.org/10.1093/aje/kwh255>
- [36] Yichen Wang, Evangelos Theodorou, Apurv Verma, and Le Song. 2016. A Stochastic Differential Equation Framework for Guiding Online User Activities in Closed Loop. (mar 2016). arXiv:1603.09021 <http://arxiv.org/abs/1603.09021>
- [37] Yichen Wang, Xiaojing Ye, Haomin Zhou, Hongyuan Zha, and Le Song. 2017. Linking Micro Event History to Macro Prediction in Point Process Models. In *Proceedings of the 20th International Conference on Artificial Intelligence and Statistics*, Vol. 54. 1375–1384. <http://proceedings.mlr.press/v54/wang17f.html>
- [38] Jiyoung Woo and Hsinchun Chen. 2016. Epidemic model for information diffusion in web forums: experiments in marketing exchange and political dialog. *SpringerPlus* 5, 1 (dec 2016), 66. <https://doi.org/10.1186/s40064-016-1675-x>
- [39] Ping Yan. 2008. Distribution Theory, Stochastic Processes and Infectious Disease Modelling. In *Mathematical Epidemiology*, Wu J. Brauer F., van den Driessche P. (Ed.). Springer, Berlin, Heidelberg, Chapter 10, 229–293. [https://doi.org/10.1007/978-3-540-78911-6\\_10](https://doi.org/10.1007/978-3-540-78911-6_10)
- [40] Linyun Yu, Peng Cui, Fei Wang, Chaoming Song, and Shiqiang Yang. 2017. Uncovering and predicting the dynamic process of information cascades with survival model. *Knowledge and Information Systems* 50, 2 (feb 2017), 633–659. <https://doi.org/10.1007/s10115-016-0955-7> arXiv:1505.07193
- [41] Damián H. Zanette. 2002. Dynamics of rumor propagation on small-world networks. *Physical Review E - Statistical, Nonlinear, and Soft Matter Physics* 65, 4 (mar 2002), 041908. <https://doi.org/10.1103/PhysRevE.65.041908> arXiv:0110324
- [42] Ali Zarezade, Abir De, Hamid Rabiee, and Manuel Gomez Rodriguez. 2017. Cheshire: An Online Algorithm for Activity Maximization in Social Networks. (mar 2017). arXiv:1703.02059 <http://arxiv.org/abs/1703.02059>
- [43] Ali Zarezade, Utkarsh Upadhyay, Hamid Rabiee, and Manuel Gomez Rodriguez. 2017. RedQueen: An Online Algorithm for Smart Broadcasting in Social Networks. In *10th ACM International Conference on Web Search and Data Mining*. arXiv:1610.05773 <http://arxiv.org/abs/1610.05773>
- [44] Qingyuan Zhao, Murat A Erdogdu, Hera Y He, Anand Rajaraman, and Jure Leskovec. 2015. SEISMIC: A Self-Exciting Point Process Model for Predicting Tweet Popularity. In *ACM SIGKDD Conference on Knowledge Discovery and Data Mining*.

## CONTENTS (APPENDIX)

A	Inter-event time probabilities in non-homogeneous Poisson processes	11
A.1	Inter-arrival times probabilities	11
A.2	Two follow-up conclusions	12
B	Fitting HawkesN with AMPL – implementation	12
B.1	AMPL introduction	12
B.2	Used solvers and optimization setup	13
B.3	Interfacing AMPL with R	13
C	Relation between deterministic SIR and stochastic SIR	13
D	SIR-HawkesN equivalence through simulation and fitting	13
D.1	Maximum likelihood estimates for SIR	13
D.2	Equivalence on Synthetic Data	14
E	Robustness of fit – additional graphics	15
F	Generalization performance – Hawkes	15

ãÄöäÖ

## A INTER-EVENT TIME PROBABILITIES IN NON-HOMOGENEOUS POISSON PROCESSES

In this section, we revisit the Non-Homogeneous Poisson Process (NHPP) and we compute the formula for the probabilities of observing inter-arrival times. We also show that NHPP is a non-Markovian process and we derive a simple proof for the formula for the log-likelihood of a NHPP, which is widely used in CS literature, but an accessible proof of which is currently missing.

### A.1 Inter-arrival times probabilities

Here we compute the probability of observing  $t_i$  – the arrival of an event. We denote by  $\tau_i$  the inter-arrival time between event  $i - 1$  and event  $i$ . It follows that  $\tau_i = t_i - t_{i-1}$  and  $t_i = \sum_{j=1}^i \tau_j$ . We study in parallel the Homogeneous Poisson Process (HPP) and NHPP. For ease of understanding, we further consider the two cases when  $i = 1$  and  $i > 1$ .

**The arrival of the first event  $t_1$ .** In a HPP of intensity  $\lambda$ , the probability of having no events in the time interval  $[0, t)$  is:

$$\mathbb{P}[t_1 \geq t] = e^{-\lambda t} . \quad (19)$$

This can be interpreted as the probability of waiting at least  $t$  units of time until the first event. Consequently, Eq. (19) is the CCDF (Complementary Cumulative Distribution Function) of the waiting time until the first event. The PDF is  $PDF = \frac{\partial}{\partial t}(1 - CCDF) = -\frac{\partial}{\partial t}CCDF$ . Consequently the waiting time to the first event in a HPP is distributed exponentially, with parameter  $\lambda$ :

$$\mathbb{P}[t_1 = t] = -e^{-\lambda t} \frac{\partial}{\partial t} = \lambda e^{-\lambda t} . \quad (20)$$

For a NHPP with the event rate  $\lambda(t)$ , we first define the function  $\Lambda(t) = \int_0^t \lambda(\tau) d\tau$ . The inverse relation between  $\lambda(t)$  and  $\Lambda(t)$  is  $\lambda(t) = \frac{\partial}{\partial t} \Lambda(t)$ . We have:

$$\mathbb{P}[t_1 \geq t] = e^{-\Lambda(t)} , \quad (21)$$

and we compute

$$\mathbb{P}[t_1 = t] = \frac{\partial}{\partial t} e^{-\Lambda(t)} = -e^{-\Lambda(t)} \frac{\partial}{\partial t} \Lambda(t) = \lambda(t) e^{-\Lambda(t)}. \quad (22)$$

Note that *the waiting time to the first event is not exponentially distributed in the case of NHPP*. An intuitive interpretation of Eq. (22) is that the probability of observing an event at time  $t$  is the product of the probability of observing an event in the infinitesimal time interval  $[t, t + \partial t]$  – equal to the event rate  $\lambda(t)$  – and the probability having observed no event in  $[0, t]$  – as defined in Eq.(21).

**The arrival of  $t_2, t_3, \dots, t_n$ .** For a HPP of rate  $\lambda$ , the probability of not observing an event in the interval  $[t, t + s]$  – after having observed a first event at time  $t_1 = t$  – is:

$$\mathbb{P}[t_2 - t_1 \geq s | t_1 = t] = e^{-\lambda(t+s-t)} = e^{-\lambda s}.$$

does not depend of  $t$ . By denoting  $\tau_2 = t_2 - t_1$  and  $\tau_1 = t_1$ , we obtain

$$\mathbb{P}[\tau_2 = s | \tau_1 = t] = \lambda e^{-\lambda s} \implies \mathbb{P}[\tau_i = s] = \lambda e^{-\lambda s}. \quad (23)$$

Inter-arrival times in a HPP are exponentially distributed with parameters  $\lambda$ , and the probability of observing a  $\tau_i$  does not depend on the previous inter-arrival times  $\tau_1, \tau_2, \dots, \tau_{i-1}$ . This property is called *memorylessness* – and it is equivalent to the Markovian property [2] – as the next state of the process depends only on the current state and not on the past.

For the NHPP of rate  $\lambda(t)$ , we have

$$\begin{aligned} \mathbb{P}[t_2 - t_1 \geq s | t_1 = t] &= e^{\Lambda(t) - \Lambda(t+s)} \\ \implies \mathbb{P}[t_2 - t_1 = s | t_1 = t] &= \frac{\partial}{\partial s} \mathbb{P}[t_2 - t_1 \geq s | t_1 = t] \\ &= \lambda(t+s) e^{\Lambda(t) - \Lambda(t+s)} \end{aligned}$$

$\Lambda(t) - \Lambda(t+s)$  can be interpreted as the minus area under the curve of  $\lambda(t)$ . We can further show that

$$\mathbb{P}[\tau_{i+1} = s | \mathcal{H}_i] = \lambda(t_i + s) e^{\Lambda(t_i) - \Lambda(t_i+s)} \quad (24)$$

where  $\mathcal{H}_i = \{t_1, t_2, \dots, t_i\}$  is the history of the process up to event  $t_i$ . Note that when  $\lambda(t) = \lambda$  – i.e. a HPP – we have  $\Lambda(t) = \lambda t$  and Eq. 23 and 24 are identical. We can express Eq. (24) in terms of event times (rather than inter-event times):

$$\mathbb{P}[t_{i+1} | \mathcal{H}_i] = \lambda(t_{i+1}) e^{\Lambda(t_i) - \Lambda(t_{i+1})} \quad (25)$$

## A.2 Two follow-up conclusions

We study the Markovian property of NHPP and we derive its likelihood function.

**NHPP is not Markovian.** One direct consequence of Eq (24) is that inter-arrival times in a NHPP are not exponentially distributed. We further study if the process is memoryless – i.e. if it has the Markovian property. For this, we compute the join probability of having an event in the interval  $[0, t]$  and a second event in  $[t, s]$ .

$$\begin{aligned} \mathbb{P}[t_1 = t, t_2 = t + s] &= \mathbb{P}[t_1 = t] \mathbb{P}[t_2 = t + s | t_1 = t] \\ &= \lambda(t) \lambda(t+s) e^{-\Lambda(t+s)} \end{aligned} \quad (26)$$

which shows that  $t_2$  is not independent of  $t_1$ . The implication is that the next state of a NHPP – i.e.  $t_{i+1}$  – is dependent on all previous states –  $t_j, j \in [1 \dots i]$ . *This shows that NHPP is not Markovian.* Note that this is a general results, for non-specific functions  $\lambda(t)$  Specific functions  $\lambda(t)$  can be constructed so that the NHPP becomes Markovian.

As a sanity check, we write Eq. (26) for a HPP. We obtain

$$\begin{aligned} \mathbb{P}[t_1 = t, t_2 = t + s] &= \lambda^2 e^{-\lambda(t+s)} \\ &= \lambda e^{-\lambda t} \lambda e^{-\lambda s} = \mathbb{P}[t_1 = t] \mathbb{P}[t_2 = t + s] \end{aligned} \quad (27)$$

therefore the inter-arrival times  $\tau_1$  and  $\tau_2$  are independent and exponentially distributed – as expected.

**The likelihood function for NHPP.** Given  $\mathcal{H}_i$ , which includes the parameter of the process  $\theta$  and the history of the process up to event  $t_i$ , the probability of an event at time  $t_{i+1}$  is defined (according to Eq. (25) as the probability of observing an event at time  $t_{i+1}$  –  $\Lambda(t_{i+1})$  – and the probability of not having observed any event in the interval  $[t_i, t_{i+1}]$ .

We construct the likelihood function as

$$\begin{aligned} \text{Likelihood}(\theta) &= \mathbb{P}[t_1, t_2, \dots, t_n | \theta] \\ &= \mathbb{P}[t_1 | \theta] \mathbb{P}[t_2 | t_1, \theta] \mathbb{P}[t_3 | t_2, t_1, \theta] \dots \mathbb{P}[t_n | t_{n-1}, \dots, t_1, \theta] \\ &= \prod_{i=1}^n \mathbb{P}[t_i | \mathcal{H}_{i-1}] = e^{-\Lambda(t_1) + \Lambda(t_1) - \Lambda(t_2) + \dots - \Lambda(t_n)} \prod_{i=1}^n \lambda(t_i) \\ &= \prod_{i=1}^n \lambda(t_i) e^{-\Lambda(t_n)} \end{aligned}$$

Finally, we derive the expression of the log-likelihood widely used in literature:

$$\begin{aligned} \log(\text{Likelihood}(\theta)) &= \sum_{i=1}^n \log(\lambda(t_i)) - \Lambda(t_n) \\ &= \sum_{i=1}^n \log(\lambda(t_i)) - \int_0^{t_n} \lambda(\tau) d\tau. \end{aligned} \quad (28)$$

## B FITTING HAWKESN WITH AMPL – IMPLEMENTATION

We fit the parameters of the HawkesN model to observed data by maximizing the log-likelihood function Eq. (28). We use AMPL, an industry standard for modeling optimization problems and with a transparent interfaces to powerful solvers. We start with an introduction of AMPL (Sec. B.1), we describe our optimization setup and the employed solvers (Sec. B.2) and we finish with the R interface that we constructed for AMPL (Sec. B.3).

### B.1 AMPL introduction

Since the first commercial release in 1993, AMPL – which stands for A Mathematical Programming Language – has provided a convenient interface between mathematic modelers and implemented solvers [11]. It now also offers a complete tool set including many solvers for modeling different optimization problems.

Our optimization problem used to involve much more than just deducing log-likelihood functions before utilizing APML. Special effort had to be expanded to derive some components because of specific requirements from solving algorithms. For example, to apply IPOPT solver to our model estimation, we were required to sketch out all parameter derivatives of log-likelihood functions and Jacobian matrix. AMPL, however, allows us to solve the problem by only defining the problem and formulating the constraints.

To run AMPL on models, it needs two parts as input including model files and data files. Model files define the problem, while

data files specify constants and initial values for variables. AMPL translator will read in those files and translate them into languages that solvers can understand. AMPL is particularly notable for its general syntax, including variable definitions and data structures.

## B.2 Used solvers and optimization setup

AMPL supports a comprehensive set of solvers including solvers for linear programming, quadratic programming and non-linear programming [10]. This link<sup>1</sup> gives a full list of solvers for AMPL.

**Solvers Applied in Implementation.** We used two solvers in our fitting procedure:

- **LGO:** a *global optimizer* for non-linear problems, which is capable of finding approximate solutions when the problems have multiple local optimal solutions ([26]). This is also one of the default solvers provided by AMPL.
- **IPOPT:** an open-source large-scale *local optimizer* for non-linear programming, which is released in 2006 [34].

Local solvers rely on improving an existing solution, employing complex techniques to avoid getting stuck in local minima. They require an initial point from which to start exploring the space of solutions. Global solvers attempt to search for the optimal solution in the entire space of solutions (one solution would be, for example, to divide the solution space into hyper-squares and apply local optimization in each one of them). Global solvers tend to find solutions which are not too far from the optimal, but they lack the precision of specialized local solvers. In summary: local solvers achieve solutions very close to the optimal, but run the risk of getting stuck in horrible local optima; global solvers achieve imprecise solutions close to the optimal.

**Optimization implementation setup.** Our optimization setup is constructed to account for the weaknesses of each class of solvers. A classical solution to the problem of local optima with local solvers is to repeat the function optimization multiple times, from different starting points. We generate 8 random sets of initial parameters, within the definition range of parameters, and we use the IPOPT solver using each of these as initial point. We also combine the global and the local solver: we use LGO to search in the space of solutions for an approximate solution, which we feed into IPOPT as initial point for further optimization. Lastly, we run IPOPT without any initial parameters, leveraging IPOPT's internal strategy for choosing the starting point based on the parameters' range of definition. After completing these 10 rounds of optimization, we select the solution with the maximum training log likelihood values. This tends to be the combination of global and local optimizer (LGO + IPOPT).

## B.3 Interfacing AMPL with R

Our entire code base is using the R language, but AMPL has its own modeling language. Therefore, we need to interface between R and AMPL. Inspired by a blog post<sup>2</sup>, we implemented our own interface between AMPL and R language. The core ideas are described as follow:

- **Generating model files and data files:** one of the major components of this interface is to generate temporary model and data files, which express the problem to be solved and the used data into AMPL language. As our experiments involve a large amount of cascades, we prefixed all temporal files with process ids so that running AMPL in parallel becomes possible.
- **Interacting with AMPL:** this is also implemented by file I/O in the disk. After model files and data files are generated, we call AMPL via system commands through R and AMPL will then start optimization. Selections of solvers can be specified in the system commands used for starting AMPL. Optimization results will be saved in result files and our interface will extract results and return them.
- **Exception handling:** this is another important component of this interface as solvers are easily encountering errors during optimization process (such as computing  $\log(0)$ ) when float number running out of precision.

## C RELATION BETWEEN DETERMINISTIC SIR AND STOCHASTIC SIR

Allen [2] analyzes in details the relation between the deterministic SIR and the stochastic SIR and shows that the mean behavior of the stochastic version converges asymptotically to the deterministic version. She shows that the mean of the random function  $I(t)$  in the stochastic SIR epidemic process is less than the solution  $I(t)$  to the deterministic differential equation in Eq.(17). We study the equivalence of the two flavors of SIR through simulation. We simulate 100 realizations of the stochastic SIR and the deterministic SIR from the same set of parameters. Fig. 8 shows the sizes of the population of Susceptible  $S(t)$ , Infected  $I(t)$ , Recovered  $R(t)$  and the cumulated infected  $C_t$ . For the stochastic version, we show the median and the 2.5% / 97.5% percentiles. This result complements the analysis in Sec. 3.1.

## D SIR-HAWKESN EQUIVALENCE THROUGH SIMULATION AND FITTING

In this section, we show through simulation the equivalence of HawkesN and SIR on synthetic data. In Sec. D.1, we sketch the fitting procedures for SIR using maximum likelihood. In Sec. D.2, we perform a set of experiments of synthetic data: we demonstrate empirically through simulation and subsequent parameter fitting the equivalence between HawkesN and SIR, and we study some of their key quantities.

### D.1 Maximum likelihood estimates for SIR

The parameters of both of the flavors of SIR described in Sec. 3.1 – deterministic and stochastic – can be fitted from observed data using a maximum likelihood procedure. In the rest of this section, we describe the observed data and we derive the likelihood functions for each model.

**Likelihood function for stochastic SIR.** The SIR process is defined by the three parameters  $\{\beta, \gamma, N\}$  and it can be seen as a marked point process observed a set of events  $\{c_j, t_j, j = 1, \dots, n\}$ , where  $c_j$  is the class of event  $t_j$  (infection or recovery). The likelihood of observing a particular event  $\{c_j, t_j\}$  has two components:

<sup>1</sup><http://www.ampl.com/solvers.html>

<sup>2</sup><https://www.rmetrics.org/Rmetrics2AMPL>



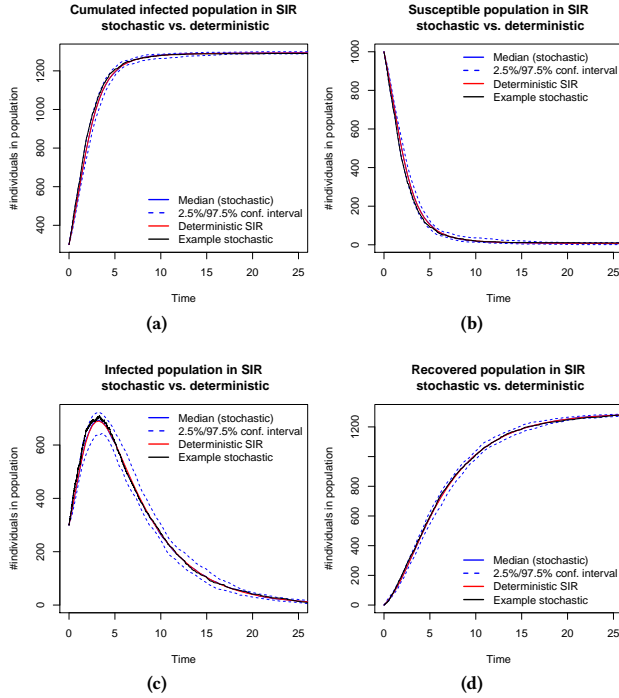


**Figure 8:** We simulate 100 stochastic SIR realizations using the parameters  $N = 1300, I(0) = 300, \beta = 1, \gamma = 0.2$ . We show the median and the 2.5% and 97.5% percentile and the deterministic evolution simulated with the same parameters. We also show an example of stochastic realization.

the likelihood of observing the inter-arrival time  $\Delta t_j = t_j - t_{j-1}$  (note that  $\Delta t_j$  is different from  $\tau_j$ , the time to recovery defined in Sec. 3.1); the likelihood of observing an event of that particular class. The event rate of the point process is  $\lambda(t) = \lambda^I(t) + \lambda^R(t)$  (defined in Lemma 3.2), which is piece-wise constant between events (shown in Fig. 2). Consequently, the likelihood of observing an inter-arrival time  $\Delta t_j$  is  $\lambda(t_{j-1})e^{-\lambda(t_{j-1})\Delta t_j}$ . Finally, the probability of observing the given class of event is given by Eq. 18. Formally, the likelihood function for the stochastic SIR is:

$$\begin{aligned} \mathcal{L}(\beta, \gamma, N) = & \prod_{j=2}^n \left[ \lambda(t_{j-1}) e^{-\lambda(t_{j-1})(t_j - t_{j-1})} \right] \\ & \times \prod_{j=2}^n \left[ \frac{\beta S(t_{j-1})}{\beta S(t_{j-1}) + N\gamma} \mathbb{1}(c_j = \text{"infection"}) \right] \\ & \times \prod_{j=2}^n \left[ \frac{N\gamma}{\beta S(t_{j-1}) + N\gamma} \mathbb{1}(c_j = \text{"recovery"}) \right] \end{aligned} \quad (29)$$

We minimize the negative logarithm of the function in Eq. (29) using L-BFGS-B [21] with the parameter bounds  $\beta > 0, \gamma > 0, N > n$ .

**Likelihood function for deterministic SIR.** Unlike HawkesN and the stochastic SIR, the deterministic SIR observes volumes of population at discrete time intervals  $\{S[t], I[t], R[t]\}$ ,  $t = t_1, t_2, \dots, S[t], I[t]$  and  $R[t]$  are time-series. The key to fitting the parameters of the deterministic SIR ( $\{\beta, \gamma, N\}$ ) is constructing the predicted

**Table 2: Equivalence of Hawkes and SIR through simulation. All parameters are shown as SIR parameters.**

parameters	N	$\gamma$	$\beta$
simulation (ideal)	1300.00	0.20	1.00
SIR $\rightarrow$ HawkesN	$1300.2 \pm 8.7$	$0.19 \pm 0.04$	$0.95 \pm 0.05$
HawkesN $\rightarrow$ SIR	$1311.23 \pm 28.16$	$0.23 \pm 0.09$	$1.01 \pm 0.08$

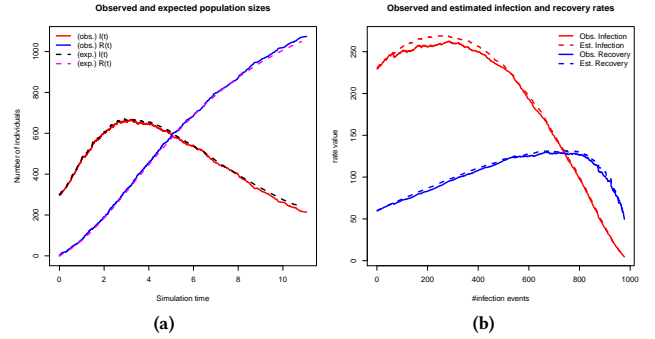


**Figure 9:** (a) Observed (continuous lines) and expected (dashed lines) sizes of **infected population** ( $I(t)$  and  $\mathbb{E}_{\tau_j}[I(t)]$ ) and **recovered population** ( $R(t)$  and  $\mathbb{E}_{\tau_j}[R(t)]$ ); (b) Observed (continuous lines) and expected (dashed lines) **rate of new infections** ( $\lambda^i(t)$  and  $\mathbb{E}_{\tau_j}[\lambda^i(t)]$ ) and **rate of new recoveries** ( $\lambda^r(t)$  and  $\mathbb{E}_{\tau_j}[\lambda^r(t)]$ ). SIR simulated with parameters:  $N = 1300, I(0) = 300, \beta = 1, \gamma = 0.2, R_0 = 5$ .

time-series  $\bar{S}[t], \bar{I}[t], \bar{R}[t]$  by simulating forward the system of differential equations (8)-(10) starting from  $\bar{S}[0] = N - I(0), \bar{I}[0] = I(0), \bar{R}[0] = 0$ . Finally, we either minimize a square error loss metric, or we construct a likelihood metric starting from the observation that the random variable counting the number of events in a Poisson process is Poisson distributed.

## D.2 Equivalence on Synthetic Data

We study the equivalence of HawkesN and SIR on synthetic data, through simulation and fitting. We simulate 20 realizations of the stochastic SIR model using a fixed set of parameters. For each realization, we fit the new infection process  $t_j^I$  using HawkesN, following the procedure shown in Sec. D.1. The HawkesN parameters are mapped into SIR parameters using Theorem 3.1. We present in Table 2 the mean and standard deviation for each fitted parameter. We also perform the inverse operation: we simulate 20 realization of a HawkesN process using the same (equivalent) previous parameters. Because the recovery times are not observed, the likelihood corresponding to the inter-arrival times  $\Delta t_j$  (first term on the r.h.s. of Eq. 29) is not defined and we cannot fit a stochastic SIR process. However, we can fit a deterministic SIR by computing population sizes ( $S(t)$  and  $C(t) = I(t) + R(t)$ ) at fixed intervals of time. Table 2 shows the mean and standard deviation of the fitted parameter. Visibly, the fitted parameters are very close to the simulation parameters, in accordance with the theoretical results in Sec. 3.2.

Fig. 9a shows the relation between observed and expected SIR population sizes ( $I(t)$  and  $\mathbb{E}_\tau[I(t)]$ ;  $\lambda^I(t)$  and  $\mathbb{E}_\tau[\lambda^I(t)]$ ), for one SIR stochastic realization. We can see that the expectation traces closely the observed values. Similar conclusions can be drawn from Fig. 9b, for the observed infection and recovery rate ( $\lambda^I(t)$  and  $\lambda^R(t)$ ) and their expectation when only the new infection events are observed ( $\mathbb{E}_\tau[\lambda^I(t)]$  and  $\mathbb{E}_\tau[\lambda^R(t)]$ ).

## E ROBUSTNESS OF FIT – ADDITIONAL GRAPHICS

Fig. 10 shows the robustness of fit for parameters  $\kappa$ ,  $\beta$  and  $\theta$  for Hawkes (a)-(c) and HawkesN (d)-(f). This result complements Sec. 5.1.

## F GENERALIZATION PERFORMANCE – HAWKES

Fig. 11 shows the generalization performance of Hawkes, for increasing amounts of data. Each cascade in a random sample of 1000 cascades in News is observed for increasing periods of time. This result complements the analysis in Sec. 5.3.

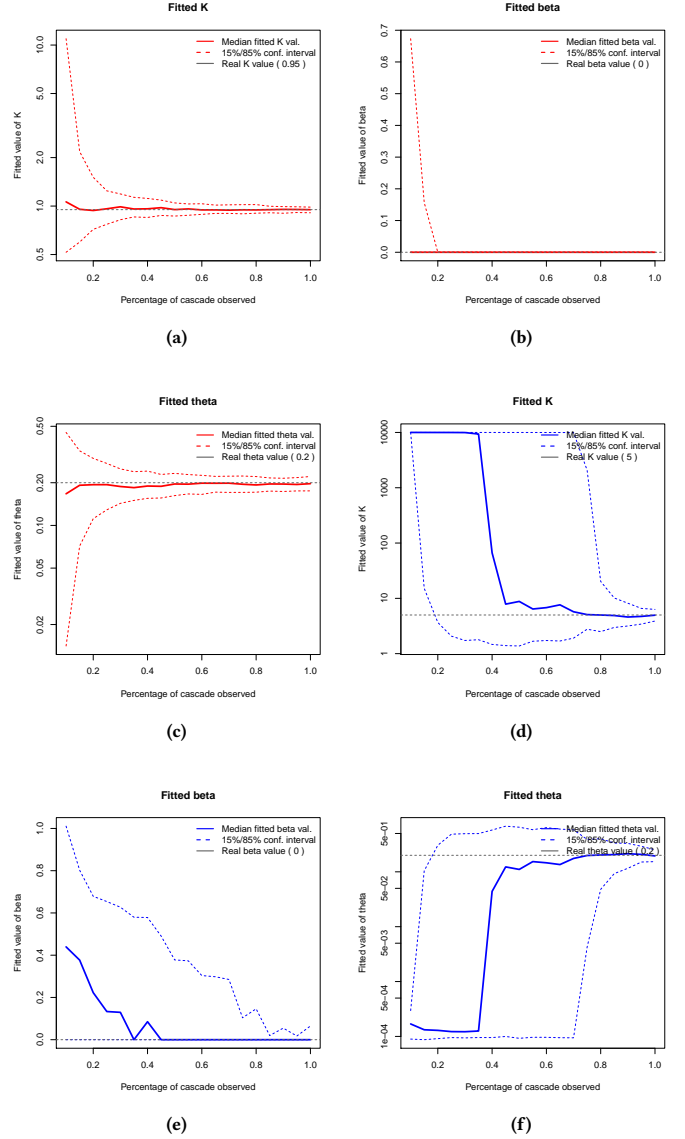


**Figure 10: Robustness of estimating parameters  $\kappa$ ,  $\beta$  and  $\theta$  for Hawkes (a)-(c) and HawkesN (d)-(f). One set of parameters for each model was simulated 100 times and fitted on increasingly longer prefixes of each simulation. One value for parameter is obtained for each fit and the median and the 15%/85% percentile values are shown.**

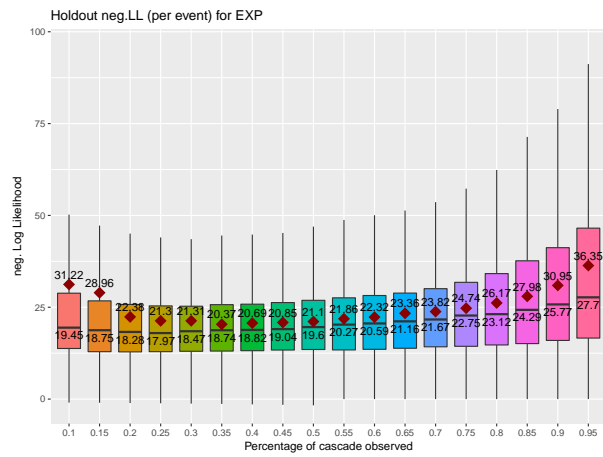


**Figure 11: Performances of Hawkes explaining unobserved data, using holdout negative log likelihood. The performance over 1000 randomly sampled cascades in NEWS are summarized using boxplots, lower is better. The percentage of observed events in each cascade used to train Hawkes is varied between 10% and 95%.**